

Realistic many-body theory of Kondo insulators: Renormalizations and fluctuations in $\text{Ce}_3\text{Bi}_4\text{Pt}_3$

Jan M. Tomczak^{1,*}

¹*Institute for Solid State Physics, TU Wien, Vienna, Austria*

(Dated: March 1, 2022)

Our theoretical understanding of heavy-fermion compounds mainly derives from iconic models, such as those due to Kondo or Anderson. While providing invaluable qualitative insight, detailed comparisons to experiments are encumbered by the materials' complexity, including the spin-orbit coupling, crystal fields, and ligand hybridizations. Here, we study the paradigmatic Kondo insulator $\text{Ce}_3\text{Bi}_4\text{Pt}_3$ with a first principles dynamical mean-field method that includes these complications. We find that salient signatures of many-body effects in this material—large effective masses, the insulator-to-metal crossover, the concomitant emergence of Curie-Weiss behaviour and notable transfers of optical spectral weight—are captured *quantitatively*. With this validation, we elucidate the fabric of the many-body state. In particular, we extend the phenomenology of the Kondo crossover to time-scales of fluctuations: We evidence that spin and charge degrees of freedom each realize two regimes in which fluctuations adhere to vastly different decay laws. We find these regimes to be separated by a *common* temperature T_χ^{max} , linked to the onset of Kondo screening. Interestingly, below (above) T_χ^{max} , valence fluctuations become faster (slower) than the dynamical screening of the local moments. Overall, however, spin and charge fluctuations occur on comparable time-scales of $\mathcal{O}(0.5 - 12 \text{ fs})$, placing them on the brink of detection for modern time-resolved probes.

PACS numbers: 71.10.-w, 71.27.+a, 75.30.Mb

Introduction.— Heavy-fermion materials[1–3] harbour a cornucopia of phenomena: the Kondo effect, spin-ordered phases, superconductivity, quantum criticality, and, potentially, topological effects. For a subclass of these system, coined Kondo insulators[4–6], the heavy mobile charges released via Kondo screening completely fill the valence bands, thus opening a charge and spin gap. Qualitatively, this behaviour can be understood, e.g., within the periodic Anderson model[7, 8]. However, oftentimes the physics in real materials is strongly influenced by ingredients not contained in reductionist models. Given the delicate competition of a multitude of energy scales in correlated materials, leaving out complexity may substantially bias the analysis[9]. Indeed, electronic structure details have been identified as crucial for understanding heavy-fermion insulators[10–13]. The most formidable challenge is to quantitatively capture the signatures of Kondo-singlet formation in spectral, optical and magnetic observables over a large temperature range[2]. Important insights have been gained under simplifying circumstances—low temperatures[11, 13], high temperatures[12], weak hybridizations[14], or strong coupling[15]—yet an unbiased description of coherence effects in $4f$ -systems still heavily relies on model calculations[16, 17][18]. Here, we spearhead realistic simulations that meet all of the above challenges for the archetypal Kondo insulator $\text{Ce}_3\text{Bi}_4\text{Pt}_3$. After analysing signatures of Kondo screening in diverse observables, we characterize the time-dependence of spin and charge relaxation processes. By establishing the magnitude of relevant time-scales, we provide essential guidelines for future applications of time-resolved probes[19–21] to Kondo insulators.

Prelude.— The cubic intermetallic compound $\text{Ce}_3\text{Bi}_4\text{Pt}_3$ is a classic Kondo insulator[5, 6, 23]: Photoemission[24] and optical[22] spectra, as well as magnetic susceptibilities[23, 25] are qualitatively consistent with the Kondo scenario[26]. Moreover, resistivity[27] and specific heat[28] measurements in high magnetic fields evidenced a collapse of the charge and spin gap—congruent with a field-induced coming asunder of Kondo singlets. Interest in $\text{Ce}_3\text{Bi}_4\text{Pt}_3$ surged by the recent proposal[29] that it may harbour topological effects associated with its non-symmorphic crystal symmetry[30]. Indeed, topological Kondo insulators[31] provide a unique playground to study the interplay of electronic correlations and topology[32][33].

Method.— Realistic many-body calculations were performed in the framework of density functional theory plus dynamical-mean field theory (DFT+DMFT)[34, 35], employing the package of Haule *et al.* [36, 37]—that combines DFT from Wien2k[38] with a continuous-time quantum monte-carlo[39] solver and includes charge self-consistency—which has previously also been applied to elemental Ce[37, 40] and Ce-compounds[36, 41, 42]. We used the PBE functional and rotationally invariant interactions parametrized by a Hubbard $U = 5.5\text{eV}$ and Hund's $J = 0.68\text{eV}$ similar to values used before[14, 36, 42–44]. Analytical continuation was done as described in Ref. [36]; optical spectra were computed as in Ref. [45].

Many-body theory: observables.— We first validate the approach by computing experimental observables. Fig. 1(a) displays the simulated local spectral function $A(\omega)$ of $\text{Ce}_3\text{Bi}_4\text{Pt}_3$: Cooling down from room temperature, a largely featureless metal evolves into a narrow-gap semiconductor with a gap $\Delta \approx 10\text{meV}$ —in con-

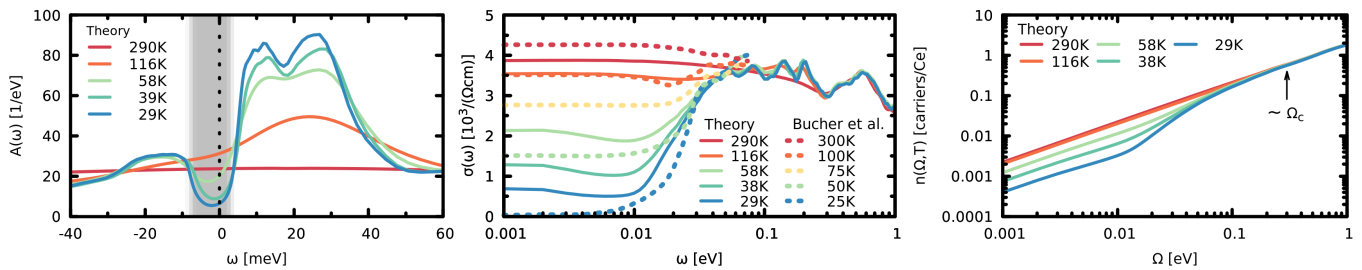


FIG. 1: (color online). Spectral and optical properties: (a) local spectral function $A(\omega)$, (b) optical conductivity $\sigma(\omega)$ (experiment from Ref. 22), (c) optical weight $n(\Omega, T) = \frac{2m}{\hbar\pi e^2} \int_0^\Omega \sigma(\omega, T) d\omega$ is recovered only for $\Omega_c \gtrsim 300\text{meV}$.

gruence with photoemission spectroscopy (see e.g., Ref. 24). Momentum-resolved spectra reveal more details: Above 100K, see Fig. 2(a), a wide band of incoherent excitations—incompatible with the notion of a Fermi surface—lingers at the Fermi level. Upon cooling, see Fig. 2(b), features outside $\pm 50\text{meV}$ sharpen, yet remain roughly at constant positions. Closer to the Fermi level, the effects are much larger: Characteristic of Kondo insulators, a charge gap Δ emerges below a temperature $T^* \sim 50\text{K}$ (cf. Fig. 1(a)) that is much smaller than the size of the gap, $\Delta/k_B \gtrsim 120\text{K}$, which itself is radically smaller than the local Coulomb repulsion U .

That our simulations capture the metal-insulator crossover in $\text{Ce}_3\text{Bi}_4\text{Pt}_3$ on a *quantitative* level is shown in Fig. 1(b) for the optical conductivity $\sigma(\omega)$: Direct comparison to experiments of Bucher *et al.*[22] reveals that, both, the absolute magnitude of the response and the energy scale of the (optical) gap that emerges at low temperatures are well reproduced. Note that the insulator-to-metal crossover is not driven by a displacement of the gap edges. Indeed, peak positions in $\sigma(\omega)$ do not move significantly with temperature. Instead, a featureless low-energy response—indicative of incoherent charge carriers—builds up with increasing T . We can analyze the evolution of the optical spectrum through the f -sum rule[46]: The integral, $n(\Omega, T) = \frac{2m}{\hbar\pi e^2} \int_0^\Omega \sigma(\omega, T) d\omega$, evaluates—for $\Omega \rightarrow \infty$ —to a temperature-independent constant: the total density of carriers participating in optical absorption. The characteristic frequency Ω_c above which $n(\Omega, T)$ becomes independent of T thus sets the energy scale over which spectral weight transfers occur as the system passes through the metal-insulator crossover. Experimentally $\Omega_c \sim 250\text{meV}$ [47], corresponding to more than five times the optical gap[22], indicative of strong correlation effects[8]. In our calculation, we capture this energy scale quantitatively, see Fig. 1(c): Indeed, the loss of low-energy spectral weight upon cooling is not recovered until above at least $\Omega_c \gtrsim 300\text{meV}$. These findings strongly support the hypothesis that states from large parts of the conduction electron bandwidth participate in the formation of Kondo singlets[2].

Many-body theory: microscopic insights.— With the above validation of the computational approach, we now analyse our results in detail. We begin with the self-energy that contains pertinent information about many-body renormalizations. We find the Ce- $4f$ -derived spectral weight at the Fermi level to be dominated by the $J = 5/2$ components, and the corresponding self-energies Σ to exhibit characteristics of a Fermi liquid: The real parts are linear at low energy, giving rise to a mass enhancement of $m^*/m = 1/Z = 1 - \partial_\omega \text{Re}\Sigma(\omega = 0) \approx 10$ for all $J = 5/2$ components. These masses are in line with the shrinking of the charge gap by one order of magnitude with respect to the DFT band-gap ($\Delta_{\text{DFT}} \approx 130\text{meV}$ [6, 48]), and are only weakly temperature-dependent. The scattering rates (inverse lifetimes) encoded in the imaginary part of the self-energy evolve quadratically with temperature[49]: $-\text{Im}\Sigma(\omega = 0) = aT^2$ for all $J = 5/2$ components, with a prefactor $a = 7.8 \cdot 10^{-3}\text{meV/K}^2$ large enough to result in a broadening $-Z\text{Im}\Sigma(0)$ of one-particle excitations in excess of $\Delta \approx 10\text{meV}$ at $T = 116\text{K}$, cf. Fig. 2 (a). These insights quantify the above claim that $\text{Ce}_3\text{Bi}_4\text{Pt}_3$ metallizes through the emergence of incoherent ($\text{Im}\Sigma$ -caused) weight at low-energies, while the fundamental gap (controlled by $\text{Re}\Sigma$) remains roughly unchanged.

We continue the analysis by looking at crucial ingredients to the here employed dynamical mean-field theory (DMFT)[34]: it maps the periodic solid onto an effective atom that can exchange particles with a bath, realizing a single-site Anderson impurity model. The effective atom is characterized by a local Hamiltonian $H^{\text{atom}} = H^{\text{loc}} + H^{\text{int}}$ (consisting of a one-particle and interacting part, respectively) and the coupling to its environment is described by an auxiliary hybridization function, $\Delta = \omega + \mu - H_{ff}^{\text{loc}} - \Sigma_{ff} - (G_{\text{loc}}^{-1})_{ff}$. Here H^{loc} , Σ and G_{loc} are the one-particle part of the atom's Hamiltonian, the impurity self-energy and the locally projected Green's function, respectively; subscripts f denote a restriction onto a subspace of correlated orbitals (here the Ce- $4f$); μ is the chemical potential. Already on the level of band-theory ($\Sigma = 0$, H^{loc} from DFT, $H^{\text{int}} = 0$), $\Delta(\omega)$ can be used to investigate *trends* in families of heavy-

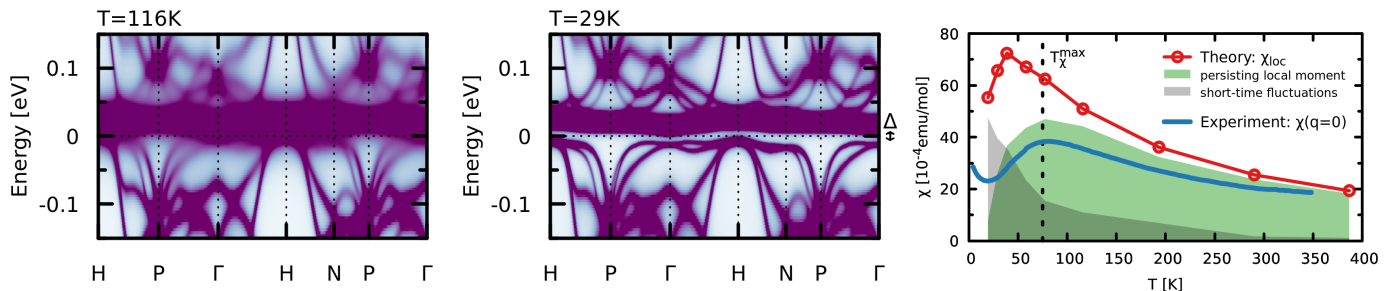


FIG. 2: (color online). Simulated momentum-resolved spectra for (a) $T = 116\text{K}$ (metallic), (b) $T = 29\text{K}$ (insulating with gap Δ). (c) Theoretical local magnetic susceptibility χ_{loc} and experimental uniform susceptibility $\chi(\mathbf{q} = 0)$ [23]. The former is decomposed via Eq. (2) into fluctuations at short-time scales and the local moment that persists for long times (see text for details). The maximum T_{χ}^{max} is a proxy for the onset of Kondo screening.

fermion materials[50, 51], e.g., regarding the degree of itineracy of $4f$ -states, the unit-cell volume or the Kondo temperature. Within DMFT, $\Delta(\omega)$ is promoted to the Weiss mean-field, which is determined self-consistently through the requirement

$$\left[\sum_{\mathbf{k}} [\omega + \mu - H(\mathbf{k}) - \Sigma_{ff}(\omega)]^{-1} \right]_{ff} = [\omega + \mu - H_{ff}^{loc} - \Delta(\omega) - \Sigma_{ff}(\omega)]^{-1} \quad (1)$$

stating that the local projection of the solid's Green's function in the subspace of correlated orbitals (l.h.s. of Eq. (1)) equals the Green's function of the impurity (r.h.s.)—when approximating the solid's self-energy $\Sigma(\mathbf{k}, \omega)$ by the impurity $\Sigma_{ff}(\omega)$ one.

By scrutinizing both H^{atom} and $\Delta(\omega)$ we can gain insight into the fabric of the many-body state realized in $\text{Ce}_3\text{Bi}_4\text{Pt}_3$ [52]. First, we analyse the probability distribution of finding the solid in an eigenstate of H^{atom} , decomposed into local quantum numbers. For example, we can distinguish atomic states according to their ($4f$) occupation N and total angular momentum J . We find that $\text{Ce}_3\text{Bi}_4\text{Pt}_3$ is dominated by states with $(N, J) = (1, 5/2)$, see Fig. 3(a): The probabilities for said states sum to above 80%. Using the atomic states and their probabilities, we can also compute expectation values of local operators $\langle \mathcal{O} \rangle$: We find that, at 29K, the impurity occupation is on average $\langle N \rangle = 1.02$ with significant deviations: $\delta N = \sqrt{\langle (N - \langle N \rangle)^2 \rangle} = 0.4$, indicating that the $4f$ -states in $\text{Ce}_3\text{Bi}_4\text{Pt}_3$ are far from being localized. The average total angular momentum is $\langle J \rangle = 2.52$, with a notable standard deviation $\delta J = 0.8$ at 29K. Similarly, we can compute instantaneous local correlators $\langle \mathcal{O}^2 \rangle := \lim_{\tau \rightarrow 0} \langle \mathcal{O}(\tau) \mathcal{O}(0) \rangle$. For example, we extract an instantaneous (disordered) moment $\mu_{inst} = g_J \sqrt{\langle J^2 \rangle} \mu_B / \hbar = g_J \sqrt{\langle j(j+1) \rangle} \mu_B \approx 2.65 \mu_B$ (using $g_{J=5/2} = 0.857$). This moment is consistent with Curie-Weiss-fits, $\mu_{eff}^2 / (3k_B T)$, to the experimental susceptibility[6, 23] at high temperature (see Fig. 2(c)) and very close to $\mu_{\text{Ce}^{3+}} = 2.54 \mu_B$, realized in isolated

Ce^{3+} ($J = 5/2$) ions. As seen in Fig. 3(a), the probability histogram is virtually independent of temperature. As a consequence also the above instantaneous expectation values hardly evolve when transitioning from the incoherent metal to the Kondo insulating regime. For example, the moment μ_{inst} increases by only 14% when cooling from 290K to 29K[53]. The experimental uniform susceptibility $\chi(\mathbf{q} = 0)$ [23] and the theoretical local magnetic susceptibility χ_{loc} , on the other hand, vary in the same temperature range by more than 50%—a salient signature of a Kondo insulator[6]: At high temperatures, see Fig. 2(c), χ_{loc} and $\chi(\mathbf{q} = 0)$ display Curie-Weiss behaviour. At intermediate temperatures, the susceptibilities peak at crossover temperatures T_{χ}^{max} and diminish upon cooling further[54]. Quite generically, in the presence of a gap Δ , $\chi(\mathbf{q} = 0)$ vanishes in an activated fashion, while $\chi_{loc}(T = 0) \propto \Delta^{-1}$ saturates. That $\chi_{loc} > \chi(\mathbf{q} = 0)$ for all temperatures indicates the dominance of Hubbard interaction-driven spin-fluctuations (see also Ref. 55). The opposite is true in Hund's-physics controlled FeSi, where $\chi_{loc} \ll \chi(\mathbf{q} = 0)$ [6].

How can we reconcile these seemingly disparate temperature evolutions: inert disordered moment μ_{inst} vs. strongly temperature dependent susceptibilities? The answer lies in the time-scales of the spin-response: We have to go beyond the *instantaneous* correlators of H^{atom} , and allow for retardation effects induced by the hybridization $\Delta(\omega)$ to the particle bath. Indeed, the static local susceptibility shown in Fig. 2(c) can be obtained by an (imaginary) time average: $\chi_{loc}(\omega = 0) = \int_0^{\beta} d\tau \chi(\tau) \propto \int_0^{\beta} d\tau \langle J_z(\tau) J_z(0) \rangle$, where $\beta^{-1} = k_B T$. The strong T -dependence in $\chi_{loc}(\omega = 0)$ under the constraint of $\partial_T \mu_{inst} \approx 0$, then points to a strongly varying relaxation of local spin-fluctuations[56]. We can provide systematic insight by deconstructing the local susceptibility[49, 57]:

$$\chi_{loc}(\omega = 0) = \beta \chi_{loc}(\beta/2) + \int_0^{\beta} d\tau [\chi_{loc}(\tau) - \chi_{loc}(\beta/2)] \quad (2)$$

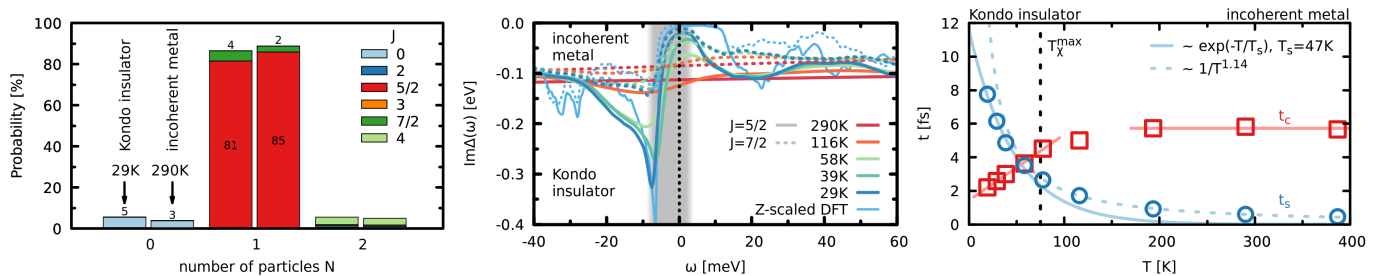


FIG. 3: (color online). Microscopic insights: (a) Effective atom description: probability to find the system in a local state with N particles and total angular momentum J . The histogram is virtually independent of temperature (left columns: 29K, right columns: 290K). (b) Hybridization function $\Delta(\omega)$: solid (dashed) lines represent the average over the $J = 5/2$ ($J = 7/2$) components. The shaded area delimits the charge gap (cf. Fig. 1(a)). For comparison the DFT hybridization functions $\Delta_0(Z\omega)$ are shown, with energies ω scaled with the quasi-particle weight $Z \approx 1/10$. (c) Time-scales t_s and t_c of magnetic screening and valence fluctuations, respectively. For both, we can distinguish two relaxation regimes separated by the common scale T_χ^{max} .

as indicated by the shaded regions in Fig. 2(c). The first term (green shaded part) describes the long-term behaviour, i.e. contributions that do not decay in time. These low-energy excitations give rise (under a probing field) to Curie-Weiss behaviour with a saturated disordered local moment. In fact, in systems with Kondo screening, the temperature dependence in the uniform susceptibility is often analysed in terms of phenomenological Curie-Weiss-law with a T -dependent effective moment: $\chi(\mathbf{q} = 0, T) = \mu_{eff}^2(T)/(3k_B T)$ [22, 49]. The latter moment approaches $\mu_{Ce^{3+}}$ in the high temperature single-ion limit as J_z becomes a good quantum number (neglecting crystal-field effects): The local f -moment is (asymptotically) unmoored from the conduction electrons' spin. Below the coherence temperature T_χ^{max} , however, Kondo screening sets in: the moment decays, approaching zero as spin excitations become gapped in the Kondo-insulating phase. Interestingly, we here observe that the contribution $\beta\chi_{loc}(\beta/2)$ of the persisting local moment to the *local* susceptibility in fact quantitatively mimics the experimental *uniform* susceptibility, see Fig. 2(c). This finding suggests to associate the empirical effective moment, $\mu_{eff}(T)$, of the uniform susceptibility with the long-term memory of the local susceptibility: $\mu_{eff}(T) = \sqrt{3\chi_{loc}(\beta/2)}$. We hence propose the computationally easier $\beta\chi_{loc}(\tau = \beta/2)$ as a proxy for $\chi(\mathbf{q} = 0, \omega = 0)$ in systems with Kondo screening.

The second contribution to $\chi_{loc}(\omega = 0)$ in Eq. (2) then describes the dynamical screening of the instantaneous moment to its magnitude persisting at large time-scales. At high temperatures, this term is small (see the grey shaded area in Fig. 2(c)) as screening is poor and μ_{eff} is close to μ_{inst} . At lower temperatures, the screened moment $\mu_{eff}(T)$ decreases while $\mu_{inst} \approx const.$, as discussed above. Thus the instantaneous moment is required to quench via efficient screening processes on short time-scales. Fitting an exponen-

tial, $\chi(\tau) = \chi(\beta/2) + [\chi(0) - \chi(\beta/2)] \exp(-\tau/t_s)$, to the short-time decay, $\tau \leq \beta/800$, we find two distinct relaxation regimes, see Fig. 3(c): If Kondo screening is absent, i.e. in the incoherent metal regime above T_χ^{max} , the characteristic time-scale t_s follows hyperbolic growth with decreasing temperature. When cooling below T_χ^{max} , however, the rise in t_s slows down and continues to grow in an activated fashion with a characteristic temperature $T_s = 47\text{K} = 4\text{meV}/k_B$, corresponding to slightly less than half of the charge and spin gap. In the low temperature limit, the screening time reaches $t_s \approx 12\text{fs}$. Indeed, in the Kondo insulating regime with spin-gap $\Delta_s \approx 12\text{meV}$ [58], high-energy fluctuations are permissible for time-scales $t_s < \hbar/(2\Delta_s) \approx 27\text{fs}$ (Heisenberg uncertainty principle). The magnitude of these fluctuations shoots up below T_χ^{max} and dominates the static local susceptibility at low enough temperatures, see Fig. 2(c). At absolute zero, this contribution is inversely proportional to the fundamental gap and, thus, the binding energy of the Kondo singlets. While we cannot give a reliable value for $\chi_{loc}(T \rightarrow 0)$, we can estimate the Kondo temperature via the Kondo lattice expression $T_K = 4T_\chi^{max}/(2J + 1)$ [59]. Using the maximum in the local-moment contribution $\beta\chi_{loc}(\beta/2)$ and $J = 5/2$, we find $T_K \approx 50\text{K}$, in agreement with previous experimental estimates[23].

The Kondo scale can also be extracted from the charge degrees of freedom: $k_B T_K = -\pi/4 \text{Im}\Delta_0 \times Z/(2J + 1)$ [59, 60]. Here Δ_0 is the unrenormalized (DFT) hybridization function, and $Z \approx 1/10$ the quasi-particle weight. Evaluating Δ_0 at its peak-position at the edge of the gap (see Fig. 3(b) and below), we find $T_K = 60\text{K}$ —in excellent congruence with the estimate from the magnetic susceptibility. The many-body hybridization function $\Delta(\omega)$ of $\text{Ce}_3\text{Bi}_4\text{Pt}_3$ itself displays a pronounced temperature dependence, see Fig. 3(b): At room temperature, $\text{Im}\Delta(\omega)$ is featureless—indicating valence fluctuations in the local-moment regime to be incoherent. In

fact, the associated time-scale, $t_c = \hbar/\text{Im}\Delta$, remains constant at ~ 6 fs throughout the incoherent metal regime, see Fig. 3(c). Upon cooling below T_χ^{max} , an increasingly sharp minimum emerges in $\text{Im}\Delta(\omega)$ at the edge of the gap. This enhancement signals the occurrence of the Kondo effect, engendering a coherent coupling between $4f$ - and conduction electron states. As a consequence, the time-scale of valence fluctuations speeds up. We find: $t_c(T) - t_c(0) \propto T$. In fact, at lowest temperatures, $\text{Im}\Delta(\omega)$ approaches the bare (non-interacting) hybridization function $\Delta_0(Z\omega)$, when accounting for the mass renormalization by scaling its energy-dependence with Z : many-body excitations resemble a (strongly renormalized) band-structure, cf. Fig. 2(b).

The hybridization function thus plays a key role in the gap-formation. In fact, on the basis of Eq. (1), we can distinguish three microscopic mechanisms for realizing an insulator, i.e. $\text{Im}G_{\text{loc}}(\omega = 0) = 0$, without broken symmetries: (i) Mott insulator: $H(\mathbf{k})$ is metallic, while $\Sigma(\omega)$ diverges inside the charge gap (Brinkmann-Rice scenario) and—as a consequence— $\text{Im}\Delta(\omega)$ is suppressed; (ii) ionic band-insulator: $H(\mathbf{k})$ is gapped by virtue of its crystal-fields H^{loc} , both Σ and Δ are well-behaved at the Fermi level; (iii) Kondo insulator: $H(\mathbf{k})$ is gapped, its crystal-fields H^{loc} are irrelevant, Σ is well-behaved but $\Delta(\omega)$ has a pronounced peak inside the gap to suppress coherent states. That the typical behaviours of the self-energy $\Sigma(\omega)$ and the hybridization function $\Delta(\omega)$ swap between a Mott and a Kondo insulator has important consequences for the time-scale of fluctuations: In their respective (incoherent) high-temperature regimes, a Mott and a Kondo insulator cannot be distinguished by looking at the magnitude of their spin and valence relaxation times [for both: $t_c \sim 10t_s \sim \mathcal{O}(10\text{fs})$]. When cooling the Mott insulator, the freezing of charge fluctuations is heralded by an increase of t_c by many orders of magnitude, while the relaxation of spins remains essentially unimpaired in the absence of a spin-gap. In this sense, spin and charge fluctuations are antagonistic, and for all T : $t_c \gg t_s$ [49]. In Kondo insulators, on the contrary, spin and charge degrees of freedom are indelibly interwoven by the Kondo effect: For example, the transferred optical spectral weight (charge) neatly correlates with the effective local moment (spin)[6, 22]. Here, we demonstrate that this tie extends also to relaxation processes: The distinct regimes of valence and spin fluctuations are both separated by the *common* scale T_χ^{max} , close to which also the hierarchy of time-scales switches ($t_s > t_c$ for $T \lesssim T_\chi^{\text{max}}$, $t_s < t_c$ for $T \gtrsim T_\chi^{\text{max}}$). Importantly, we establish that the overall time-scale of valence fluctuations in $\text{Ce}_3\text{Bi}_4\text{Pt}_3$, $t_c = 1 - 6$ fs, is close to current time-resolution limits of ultrafast X-ray spectroscopies[19, 21] as well as attosecond laser-pulse-based pump-probe measurements[20]. This suggests that monitoring the change in valence fluctuations through the Kondo crossover and the sensitivity of Kondo sin-

glet formation to external perturbations could soon be possible with time-resolved probes.

In conclusion, we computed spectral, optical and magnetic properties of $\text{Ce}_3\text{Bi}_4\text{Pt}_3$ from first principles and found excellent agreement with experiment. We then extended the phenomenology of Kondo insulators by characterizing relaxation regimes of valence fluctuations and magnetic screening. Delimiting the range of relevant time-scales, we motivated future applications of spectroscopies in the time domain, which are the next step to elucidate the many-body fabric of Kondo insulators.

Acknowledgements.— The author gratefully acknowledges discussions with S. Dzsaber, G. Eguchi, K. Held, S. Paschen, F. Steglich, and A. Toschi. This work has been supported by the Austrian Science Fund (FWF) through project “LinReTraCe” P 30213-N36.

* tomczak.jm@gmail.com

- [1] S. Wirth and F. Steglich, Nat. Rev. Materials **1**, 16051 EP (2016).
- [2] P. Coleman, in *Handbook of Magnetism and Advanced Magnetic Materials* (John Wiley & Sons, Ltd, 2007).
- [3] Q. Si and S. Paschen, physica status solidi (b) **250**, 425 (2013).
- [4] G. Aeppli and Z. Fisk, Comments Cond. Mat. Phys **16**, 150 (1992).
- [5] P. S. Riseborough, Advances in Physics **49**, 257 (2000).
- [6] J. M. Tomczak, J. Phys.: Condens. Matter (Topical Review) **30**, 183001 (2018).
- [7] M. Jarrell, H. Akhlaghpour, and T. Pruschke, Phys. Rev. Lett. **70**, 1670 (1993).
- [8] M. J. Rozenberg, G. Kotliar, and H. Kajueter, Phys. Rev. B **54**, 8452 (1996).
- [9] E.g., pioneering model studies[55, 61, 62] suggested the d -electron “flyweight”[2] Kondo insulator FeSi[6] to be controlled by Hubbard physics. Then, realistic calculations[45, 63] divulged the Hund’s rule coupling—a genuine multi-orbital effect[64]—to drive electronic correlations, explaining[6] why—instead of *local* (Curie-Weiss) moments[55, 61]—neutron experiments[65, 66] see a susceptibility enhanced at ferromagnetic wavevectors.
- [10] S. Doniach, C. Fu, and S. Trugman, Physica B: **199-200**, 450 (1994).
- [11] A. B. Shick, L. Havela, A. I. Lichtenstein, and M. I. Katsnelson, Scientific Reports **5**, 15429 EP (2015).
- [12] P. Wissgott and K. Held, Eur. Phys. J. B **89**, 5 (2016).
- [13] Y. Xu, C. Yue, H. Weng, and X. Dai, Phys. Rev. X **7**, 011027 (2017).
- [14] J. M. Tomczak, L. V. Pourovskii, L. Vaugier, A. Georges, and S. Biermann, Proc. Natl. Acad. Sci. USA **110**, 904 (2013).
- [15] J. D. Denlinger, J. W. Allen, J.-S. Kang, K. Sun, J.-W. Kim, J. H. Shim, B. I. Min, D.-J. Kim, and Z. Fisk, ArXiv e-prints (2013), arXiv:1312.6637.
- [16] P. Coleman, in *Many-Body Physics: From Kondo to Hubbard*, Modeling and Simulation, Vol. 5, edited by E. K. Eva Pavarini and P. Coleman (Verlag Forschungszentrum Jülich, 2015) pp. 1–34.

- [17] C.-H. Min, F. Goth, P. Lutz, H. Bentmann, B. Y. Kang, B. K. Cho, J. Werner, K.-S. Chen, F. Assaad, and F. Reinert, *Scientific Reports* **7**, 11980 (2017).
- [18] See, however, the recent Ref. 42.
- [19] M. Hentschel, R. Kienberger, C. Spielmann, G. A. Reider, N. Milosevic, T. Brabec, P. Corkum, U. Heinzmann, M. Drescher, and F. Krausz, *Nature* **414**, 509 EP (2001).
- [20] E. Goulielmakis, Z.-H. Loh, A. Wirth, R. Santra, N. Rohringer, V. S. Yakovlev, S. Zherebtsov, T. Pfeifer, A. M. Azzeer, M. F. Kling, S. R. Leone, and F. Krausz, *Nature* **466**, 739 EP (2010).
- [21] M. Buzzi, M. Först, R. Mankowsky, and A. Cavalleri, *Nat. Rev. Materials* (2018), 10.1038/s41578-018-0024-9.
- [22] B. Bucher, Z. Schlesinger, P. C. Canfield, and Z. Fisk, *Phys. Rev. Lett.* **72**, 522 (1994).
- [23] M. F. Hundley, P. C. Canfield, J. D. Thompson, Z. Fisk, and J. M. Lawrence, *Phys. Rev. B* **42**, 6842 (1990).
- [24] Y. Takeda, M. Arita, H. Sato, K. Shimada, H. Namatame, M. Taniguchi, K. Katoh, F. Iga, and T. Takabatake, *J Electron Spectrosc* **101103**, 721 (1999).
- [25] S. Dzsaber, L. Prochaska, A. Sidorenko, G. Eguchi, R. Svagera, M. Waas, A. Prokofiev, Q. Si, and S. Paschen, *Phys. Rev. Lett.* **118**, 246601 (2017).
- [26] S. Doniach, *Physica B+C* **91**, 231 (1977).
- [27] G. Boebinger, A. Passner, P. Canfield, and Z. Fisk, *Physica B*: **211**, 227 (1995).
- [28] M. Jaime, R. Movshovich, G. R. Stewart, W. P. Beyersmann, M. G. Berisso, M. F. Hundley, P. C. Canfield, and J. L. Sarrao, *Nature* **405**, 160 (2000).
- [29] P.-Y. Chang, O. Erten, and P. Coleman, *Nature Physics* **13**, 794 EP (2017).
- [30] K. Shiozaki, M. Sato, and K. Gomi, *Phys. Rev. B* **91**, 155120 (2015).
- [31] M. Dzero, J. Xia, V. Galitski, and P. Coleman, *Annual Review of Condensed Matter Physics* **7**, 249 (2016).
- [32] R. Schaffer, E. K.-H. Lee, B.-J. Yang, and Y. B. Kim, *Rep. Prog. Phys.* **79**, 094504 (2016).
- [33] In stark contrary to Mott-Hubbard insulators in which interaction effects can severely tamper with topological protections based on single particle symmetries[67].
- [34] A. Georges, G. Kotliar, W. Krauth, and M. J. Rozenberg, *Rev. Mod. Phys.* **68**, 13 (1996).
- [35] K. Held, *Advances in Physics* **56**, 829 (2007).
- [36] K. Haule, C.-H. Yee, and K. Kim, *Phys. Rev. B* **81**, 195107 (2010).
- [37] K. Haule, *Phys. Rev. B* **75**, 155113 (2007).
- [38] P. Blaha, K. Schwarz, G.-K.-H. Madsen, D. Kvasnicka, and J. Luitz, *Vienna University of Technology, Austria* (2001), ISBN 3-9501031-1-2.
- [39] E. Gull, A. J. Millis, A. I. Lichtenstein, A. N. Rubtsov, M. Troyer, and P. Werner, *Rev. Mod. Phys.* **83**, 349 (2011).
- [40] B. Chakrabarti, M. E. Pezzoli, G. Sordi, K. Haule, and G. Kotliar, *Phys. Rev. B* **89**, 125113 (2014).
- [41] H. C. Choi, B. I. Min, J. H. Shim, K. Haule, and G. Kotliar, *Phys. Rev. Lett.* **108**, 016402 (2012).
- [42] E. A. Goremychkin, H. Park, R. Osborn, S. Rosenkranz, J.-P. Castellan, V. R. Fanelli, A. D. Christianson, M. B. Stone, E. D. Bauer, K. J. McClellan, D. D. Byler, and J. M. Lawrence, *Science* **359**, 186 (2018).
- [43] K. Held, A. K. McMahan, and R. T. Scalettar, *Phys. Rev. Lett.* **87**, 276404 (2001).
- [44] B. Amadon, S. Biermann, A. Georges, and F. Aryasetiawan, *Phys. Rev. Lett.* **96**, 066402 (2006).
- [45] J. M. Tomczak, K. Haule, and G. Kotliar, *Proc. Natl. Acad. Sci. USA* **109**, 3243 (2012).
- [46] L. Degiorgi, *Rev. Mod. Phys.* **71**, 687 (1999).
- [47] Z. Fisk, J. Sarrao, J. Thompson, D. Mandrus, M. Hundley, A. Miglori, B. Bucher, Z. Schlesinger, G. Aeppli, E. Bucher, J. DiTusa, C. Oglesby, H.-R. Ott, P. Canfield, and S. Brown, *Physica B*: **206**, 798 (1995).
- [48] K. Takegahara, H. Harima, Y. Kaneta, and A. Yanase, *Journal of the Physical Society of Japan* **62**, 2103 (1993).
- [49] For details see Supplemental Material.
- [50] H. C. Herper, T. Ahmed, J. M. Wills, I. Di Marco, T. Björkman, D. Iuşan, A. V. Balatsky, and O. Eriksson, *Phys. Rev. Materials* **1**, 033802 (2017).
- [51] J. M. Tomczak, in preparation (2018).
- [52] We only discuss the average of the $J = 5/2$ states. For properties resolved into m_J , see Ref. [49].
- [53] This situation is akin to the covalent insulator FeSi[45], but different from the ionic insulator LaCoO₃, where a temperature-dependent histogram[68] points to the occurrence of a spin-state transition.
- [54] The low- T upturn in $\chi(\mathbf{q} = 0)$ is extrinsic[58].
- [55] J. Kuneš and V. I. Anisimov, *Phys. Rev. B* **78**, 033109 (2008).
- [56] See also Refs. [69, 70] and Watzenböck *et al.* (in preparation) for the screening of local moments in iron pnictides.
- [57] S. Hoshino and P. Werner, *Phys. Rev. Lett.* **115**, 247001 (2015).
- [58] A. Severing, J. D. Thompson, P. C. Canfield, Z. Fisk, and P. Riseborough, *Phys. Rev. B* **44**, 6832 (1991).
- [59] P. Coleman, *Phys. Rev. B* **28**, 5255 (1983).
- [60] A. C. Hewson, *The Kondo Problem to Heavy Fermions* (Cambridge University Press, 1993).
- [61] C. Fu and S. Doniach, *Phys. Rev. B* **51**, 17439 (1995).
- [62] M. Sentef, J. Kuneš, P. Werner, and A. P. Kampf, *Phys. Rev. B* **80**, 155116 (2009).
- [63] J. M. Tomczak, K. Haule, and G. Kotliar, in *New Materials for Thermoelectric Applications: Theory and Experiment*, NATO Science for Peace and Security Series B: Physics and Biophysics, edited by V. Zlatić and A. Hewson (Springer Netherlands, 2013) pp. 45–57.
- [64] A. Georges, L. d. Medici, and J. Mravlje, *Annual Review of Condensed Matter Physics* **4**, 137 (2013).
- [65] G. Shirane, J. E. Fischer, Y. Endoh, and K. Tajima, *Phys. Rev. Lett.* **59**, 351 (1987).
- [66] K. Tajima, Y. Endoh, J. E. Fischer, and G. Shirane, *Phys. Rev. B* **38**, 6954 (1988).
- [67] D. Di Sante, A. Hausoel, P. Barone, J. M. Tomczak, G. Sangiovanni, and R. Thomale, *Phys. Rev. B* **96**, 121106 (2017).
- [68] V. Krápek, P. Novák, J. Kuneš, D. Novoselov, D. M. Korotin, and V. I. Anisimov, *Phys. Rev. B* **86**, 195104 (2012).
- [69] P. Hansmann, R. Arita, A. Toschi, S. Sakai, G. Sangiovanni, and K. Held, *Phys. Rev. Lett.* **104**, 197002 (2010).
- [70] A. Toschi, R. Arita, P. Hansmann, G. Sangiovanni, and K. Held, *Phys. Rev. B* **86**, 064411 (2012).